JOURNAL OF MATERIALS SCIENCE 39 (2004) 5785–5797

Post-densification behavior of reaction-bonded silicon nitride (RBSN): Effect of various characteristics of RBSN

XINWEN ZHU, YOU ZHOU, K. HIRAO
Advanced Manufacturing Research Institute, National Institute of Advanced Industrial Science and Technology (AIST), 2268-1 Shimo-Shidami, Moriyama-ku, Nagoya 463-8687, Japan
E-mail: x-zhu@aist.go.jp

The effects of the various characteristics of reaction-bonded silicon nitride (RBSN), such as crystalline secondary phases, residual Si, pore size distribution, and agglomerates developed during nitridation on the post-densification behavior, were investigated in detail. A model experiment was carried out to study the effect of crystalline secondary phases in RBSN on the post-densification. The result clearly indicates that the pre-formation of crystalline secondary phases does not influence the sintering of Si_3N_4-powder compacts, which is further demonstrated in the post-densification of RBSN, because the formation of a liquid, including its composition and properties, is dependent on the composition of the system and sintering temperature, but independent of the presence of crystalline secondary phases. In particular, the complete melt of crystalline secondary phases is not related to their melting points and only relies on the composition of the system. The residual Si and pore size distribution in RBSN show no significant effect on the post-densification. Some large pores of $\sim$5 μm in size could be eliminated by liquid filling and grain growth during post-sintering. The residual Si in RBSN could change into β-Si_3N_4 by nitridation of liquid Si and contribute to the weight gain during the early stage of post-sintering. However, it is shown that the agglomerates in RBSN play an important role in the post-densification. The effect of agglomerates on the post-densification strongly depends on their size and amounts in RBSN. Nearly complete densification of RBSN could be reached through lowering of the nitriding temperature or adding Si_3N_4 powder to green bodies, which leads to the formation of more uniform microstructure during nitridation. A mechanism that explains how the agglomerates affect the post-densification of RBSN was discussed based on the theories of liquid phase sintering.

1. Introduction

Recently, much attention has been paid to post-sintering of reaction-bonded silicon nitride (RBSN) [1–10]. Compared with sintering of Si_3N_4-powder compacts, the sintered RBSN (SRBSN) not only has an advantage of low cost resulting from lower raw materials costs and lower costs of machining due to the lower sintering shrinkage and minimum distortions during post-sintering, but also it can be produced in complex shaped components with near-net-shape capability and with good mechanical properties similar to those of HPSN or SSN.

Because of a high degree of covalent bonding (70%), the densification of Si_3N_4 requires sintering aids and proceeds via a liquid-phase sintering mechanism [4, 11, 12]. The sintering aids used for the sintering of RBSN are similar to those applied in sintered and hot-pressed Si_3N_4, such as Al_2O_3, MgO and rare-earth oxides. The most popular method of introducing the sintering aids to the RBSN materials is to add them to the Si powder prior to nitriding and this will influence the nitriding process, post-densification and the resulting microstructure. One of the outstanding features is that the sintering aids result in the formation of crystalline secondary phases during nitridation. Kleebe *et al.* [5, 13] stressed that besides micropore size distribution, the crystalline secondary phases in RBSN play an important role in the post-densification and inhibit the post-densification. In addition, the inhomogeneous distribution of these crystalline secondary phases also results in the growth of large elongated β-Si_3N_4 crystals during the post-sintering. They proposed two reasons why the crystalline secondary phases inhibit the post-densification of RBSN. One is that the pre-formation of crystalline secondary phases results in a decrease of the amount of liquid phases. The other is that the crystalline secondary phases with a high thermal stability only dissolve, and thus

a homogeneous liquid present at rather high sintering temperature.

Recently, the melting points of crystalline $Y_4Si_2O_7N_2$ (J-phase) and $Y_{20}Si_{12}O_{48}N_4$ (H-phase) were reported to be 1880 and 1700–1800°C by Nishimura *et al.* [14]. This means that the J-phase possesses a higher melting temperature than the H-phase. Most importantly, H-phase and J-phase both should completely melt at a high sintering temperature, such as 1920°C. Dressler *et al*. [15] showed that the inhomogenously distributed crystalline secondary phases in RBSN do not result in the exaggerated grain growth because a rapid homogenization of locally formed liquid occurs via capillary forces during post-sintering at higher temperature. Hence, up to now, the role of crystalline secondary phases in the post-densification of RBSN is not clear. The influences of other characteristic factors developed during nitridation on the post-densification of RBSN have not been systematically studied. Therefore, further investigations on the post-densification behavior of RBSN are needed.

The objective of this work is to investigate the effects of various characteristic factors of RBSN on the post-sintering behavior of RBSN. The system of Yb_2O_3-MgO was chosen as the sintering aid because of several considerations. First, this system has been employed to successfully obtain dense Si_3N_4 ceramics by gas-pressure sintering of Si_3N_4-powder compacts [16, 17]. Second, the melting point of crystalline $Yb_4Si_2O_7N_2$ was determined as 1870°C [14] and was regarded as a typical crystalline secondary phase with high melting point [18, 19]. Finally, the formation of $Yb_4Si_2O_7N_2$ is almost independent of the properties of starting raw materials, additive composition, and even fabrication techniques, unlike Y_2O_3-system [16, 18, 20, 21]. No model experiment verifying the effect of crystalline secondary phases on the post-densification of RBSN has been reported to date. Thus, a model experiment based on the sintering of Si_3N_4-powder compacts was performed. Effects of various characteristic factors of RBSN, such as crystalline secondary phases, residual Si, micropore and agglomerated structure developed during nitridation on the post-densification of RBSN, were investigated in detail. The role of crystalline secondary phases in the post-densification of RBSN was clearly clarified and it is suggested that the agglomerates in RBSN plays a crucial role in the post-densification.

2. Experimental procedure

The starting materials used in this study were as follows: Si (purity $> 99\%$, $d_{50} = 1\ \mu$m, High purity chemicals, Saitama, Japan), α-Si_3N_4 powder (SN E-10, specific surface area 9–13 m^2/g, β-phase of 0.23%, oxygen content <2.0 wt%, UBE Industries, Ltd., Yamaguchi, Japan), Yb_2O_3 (purity >99.9%, specific surface area of 19.3 m^2/g, Nihon Yttrium Co. Ltd., Tokyo, Japan) and MgO (1000A, UBE Industries, Ltd., Japan). SEM photograph of the original Si powder was shown in Fig. 1. Two kinds of powder mixtures used for the preparation of RBSN materials having a Si:Si_3N_4 mass ratios of 1:0 and 5:1 were designated as RB1 and RB2, respectively. The concurrent addition of Yb_2O_3 and MgO was used as sintering aids. The only difference in the compositions of RB1 and RB2 green bodies is that the former did not contain α-Si_3N_4 particles and the latter contained Si_3N_4 particles. After full nitridation, the fraction of added α-Si_3N_4 particles is about 11% of the total weight of Si_3N_4 in the RB2 materials. The final composition of these RBSN materials after fully nitriding and sintering was designed to be 90 mol%Si_3N_4-5 mol%Yb_2O_3-5 mol%MgO. Si_3N_4-powder compacts with the same composition as RBSN materials were also prepared.

All powder mixtures were prepared by wet mixing in a planetary mill for 1 h in a Si_3N_4 jar with Si_3N_4 balls, using methanol as a mixing medium in the absence of a binder. The slurry was dried using a rotary evaporator at a temperature of 60°C, subsequently dried at 110°C

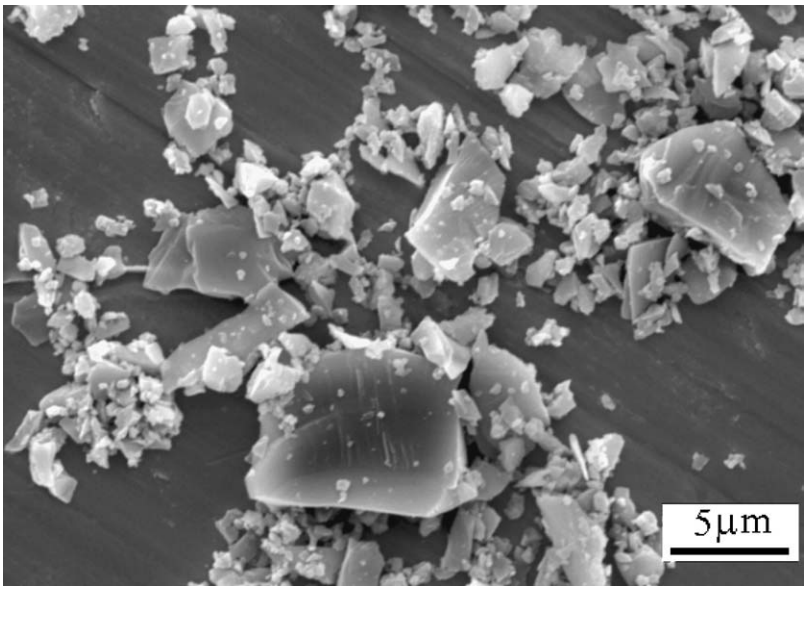

Figure 1 SEM photograph of the original Si powder used in this work.

for at least 4 h in vacuum and sieved through 100 mesh screen. Two grams of powder mixture was uniaxially pressed in a 20 mm diameter stainless steel die and then cold isostatically pressed. The cold isostatic pressure used for Si:Si_3N_4 compacts and Si_3N_4-powder compacts was 300 MPa and 400 MPa, respectively.

The nitridation of Si:Si_3N_4 green compacts was carried out in an alumina tube furnace (60 mm in diameter, Koyo Thermo System Co., Tenri-shi, Japan) with 1 L/min high purity nitrogen flow at three different temperatures: 1300°C × 16 h, 1325°C × 16 h and 1350°C × 8 h. In order to examine the effect of crystalline secondary phases on the post-densification of RBSN materials, a model experiment was conducted based on the sintering of Si_3N_4-powder compacts. Some of Si_3N_4-powder compacts were treated in the alumina tube furnace at 1350°C for 8 h and thus crystalline secondary phases were formed during this process. The sintering of the nitrided compacts and Si_3N_4-powder compacts without and with heat treatment was conducted inside a triple crucible arrangement which consisted of a double BN crucible and an outer graphite crucible in a graphite resistance furnace (Multi-500, Fujidempa Kogyo Co. Ltd., Japan) at 1800 and 1900°C with 6 h hold under a N_2 pressure of 0.1 MPa (pressureless sintering) and 1 MPa (gas-pressure sintering), respectively. The samples were placed inside an inner BN crucible with a BN powder bed (GP grade, Denki Kagaku Kogyo Co., Japan) in the double BN crucible arrangement.

The extent of nitridation was determined by the ratio of the observed weight gain and theoretical weight gain according to the reaction ($3Si \rightarrow Si_3N_4$). Linear shrinkage (LS) and volume shrinkage (VS) were determined by the apparent dimensional change of disk samples during nitridation and post-sintering. Weigh loss (WL) during post-sintering was determined by the apparent weight change of samples before and after sintering. Bulk density (BD) of the nitrided and sintered materials was measured by the Archimedes method using distilled water as an immersion medium. Theoretical density (TD) of sintered RBSN materials and Si_3N_4-powder compacts was estimated based on their designed compositions 90 mol%Si_3N_4-5 mol%Yb_2O_3-5 mol%MgO by the rule of mixture. Relative density (RD) was given by BD/TD.

The pore size distribution of the nitrided materials was determined by mercury porosimeter (Model Poremaster GT 33-1, Quantachrome Co. Ltd., Japan). The phase analysis of the nitrided and sintered materials was conducted on the cross-sections of the bulk samples by using X-ray diffractometry (XRD) (Model RINT 2500, Rigaku Co., Tokyo, Japan, Cu K_α radiation, scanning range of $2\theta = 10$–70°, operating conditions of 40 kV and 100 mA). The quantitative analysis of α- and β-Si_3N_4 of the nitrided products was performed using the method [22] described by Pigeon and Varma (scanning rate: 0.5° 2θ/min). The α-Si_3N_4 crystallite diameter (D) of the nitrided bodies was estimated from the (201) peak by the Scherrer equation:

$$D = \frac{0.89\lambda}{B\cos\theta} \quad (1)$$

where λ is the wavelength ($\lambda = 1.5406$ Å), B is the peak broadening of the crystallite diameter (D) at half of its maximum intensity, θ is the peak position.

The microstructures of the nitrided bodies were characterized by observing the fracture surfaces, which had been coated with a 30 nm layer of gold, using scanning electron microscopy (SEM) (Model JSM–5600, Jeol, Tokyo, Japan). Cross sections of sintered samples were polished with a 1 μm diamond slurry and plasma-etched in a CF_4 gas of 30 ml/min for 120 s in a commercial plasma etching apparatus (Model PR31Z, Yamato Scientific, Tokyo, Japan). The etched surfaces were observed by SEM.

3. Results

3.1. Model experiment based on the sintering of Si_3N_4-powder compacts

Table I gives the characteristics of Si_3N_4-powder compacts before and after heat treatment at 1350°C for 8 h. During heat treatment, the compacts show no significant change in the density, which is in good agreement with almost "zero" shrinkage occurring (only 0.66%). The β-phase content shows a slight increase from 0.23 to 1.65 wt% after heat treatment and this implies that the phase transformation of α to β which occurs at 1350°C was due to the formation of some liquid phase; this means that the lowest eutectic temperature in the system of Si_3N_4-SiO_2-Yb_2O_3-MgO is most likely less than 1350°C. XRD pattern of Si_3N_4-powder compacts after heating treatment shown in Fig. 2 shows that crystalline $Yb_4Si_2N_2O_7$ was the only crystalline secondary phases formed during heat treatment. The formation of $Yb_4Si_2N_2O_7$ is attributed to the following

TABLE I Characteristics of Si_3N_4-powder compacts before and after heat treatment at 1350°C for 8 h

Before heat treatment			After heat treatment				
$\beta/(\alpha+\beta)$ (wt%)	BD (g/cm^3)	RD (%)	$\beta/(\alpha+\beta)$ (wt%)	BD (g/cm^3)	RD (%)	LS (%)	OP[a] (%)
0.23	1.86	53.10	1.65	1.90	54.25	0.66	45.19

[a]OP = open porosity.

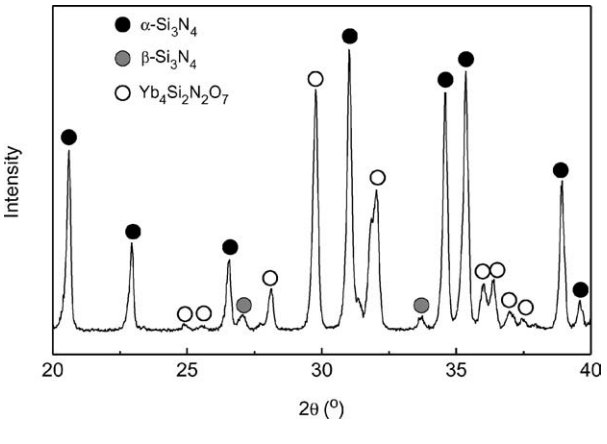

Figure 2 XRD pattern of Si_3N_4-powder compact after heat treatment at 1350°C for 8 h.

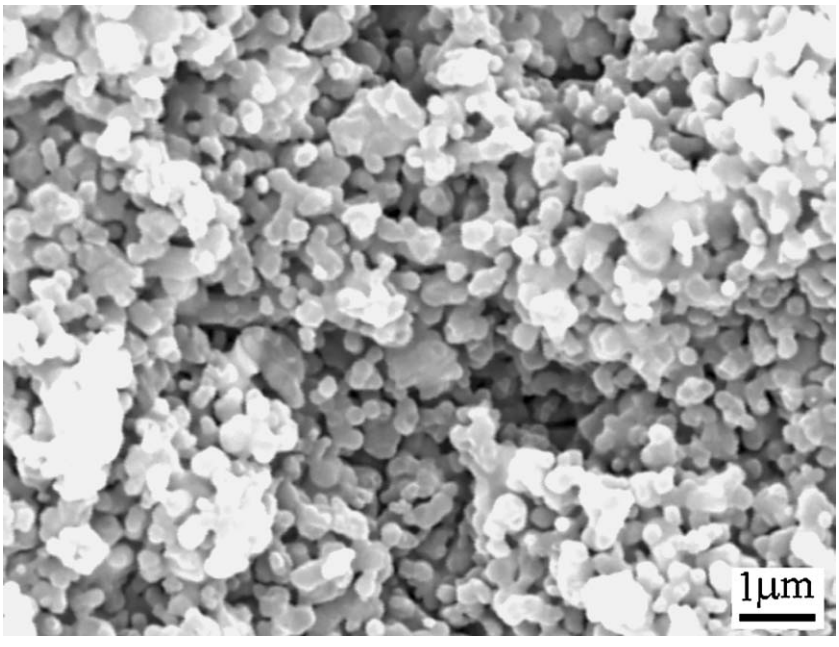

Figure 3 SEM photograph of fracture surface of Si_3N_4-powder compacts with heat treatment at 1350°C for 8 h.

solid-reaction at 1350°C:

$$Si_3N_4 + 4Yb_2O_3 + SiO_2 \rightarrow 2Yb_4Si_2N_2O_7 \qquad (2)$$

Fig. 3 shows the microstructure of Si_3N_4-powder compacts after heat treatment at 1350°C for 8 h. It is found that the Si_3N_4 grains remain fine and equiaxed, being almost the same as the starting powder. It can be concluded that this aspect of the microstructure of treated Si_3N_4-powder compacts is identical to that of those without treatment (green compacts). Thus, provided that there is a difference in the sintering behavior of Si_3N_4-powder compacts without and with heat treatment, this difference should be caused by the crystalline $Yb_4Si_2N_2O_7$ phase.

Fig. 4 illustrates the effect of pre-formation of crystalline secondary phases on the sintering of Si_3N_4-powder compacts. It is found that there is nearly no difference between the sintered densities of compacts without and with heat treatment, whether at 1800 or 1900°C. They both are sintered to more than 98% theoretical density at 1900°C. The SEM photographs shown in Fig. 5 reveal that, the microstructural development of the sintered samples without (Fig. 5a) and with heat treatment (Fig. 5b) is almost identical. Although the β-phase content shows a small increase, no significantly abnormal grain growth is observed in the sintered samples with heat treatment (Fig. 5b), which is in good agreement with the results reported by Dressler *et al.* [15] because the growth of elongated Si_3N_4 grains depends not only on the amounts β-Si_3N_4 nuclei, but also on the grain-size distribution of β-Si_3N_4 nuclei. This experiment clearly illustrates that the pre-formation of crystalline secondary phases has no effect on the sintering behavior of Si_3N_4. In the case of using Y_2O_3-Al_2O_3 system as sintering additives, Kim *et al.* [23] reported that the untreated Si_3N_4-powder compacts showed almost the same sintering behavior as those treated at 1450°C for 10 h under flowing N_2 gas, which leaded to the formation of crystalline $Y_2Si_2O_7$ phase, using α-Si_3N_4 powder (SN E-10) as the starting materials. This is in excellent agreement with our present result. Therefore, it can be concluded that crystalline secondary phases do not influence the post-densification of RBSN.

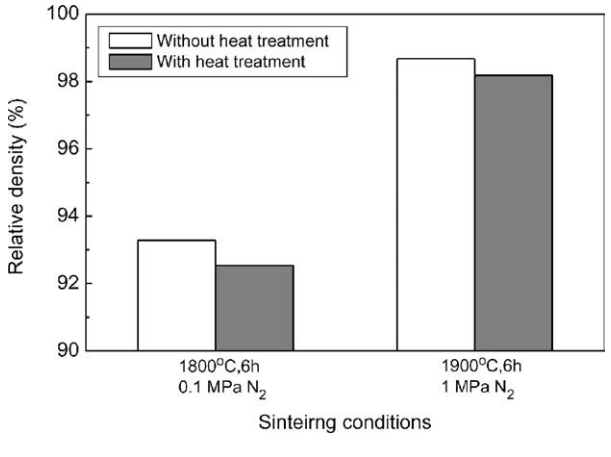

Figure 4 Effect of the pre-formation of crystalline secondary phases on the relative density of sintered Si_3N_4-powder compacts at 1800°C (pressureless sintering) and 1900°C (gas-pressure sintering).

3.2. Characteristics of RBSN materials

Table II gives the extent of nitridation, β-phase content, density, and linear shrinkage and open porosity all RBSN materials obtained at various nitriding conditions. The extent of nitridation, density and open porosity of RB1 materials decrease with the decrease of nitriding temperature. No Si peaks is detected by XRD in nitrided RB1 materials at 1350°C for 8 h, indicating complete nitridation. But, nitrided RB1 materials at 1300°C contain more residual Si owing to the lower degree of nitridation. The nitridation of sample RB1 was also carried out at 1350°C for 16 h, but the open porosity was found to be almost the same as that for

TABLE II Characteristics of all RBSN materials obtained at various nitriding conditions

Sample no.	Nitriding condition	Nitridation (%)	$\beta/(\alpha+\beta)$ (wt%)	D^c (nm)	BD (g/cm^3)	LS (%)	OP (%)
RB1	1300°C, 16 h	87.89[b]	1.11	35	2.47	2.17	15.49
	1325°C, 16 h	93.43[b]	0.75	–	2.53	2.10	16.10
	1350°C, 8 h	94.54[a]	1.65	41	2.55	1.92	20.41
RB2	1350°C, 8 h	93.62[a]	0.53	38	2.47	1.92	24.57

Note: [a]Si peak cannot be detected by XRD; [b]Si peak can be detected by XRD; [c]The diameter of α-Si_3N_4 crystallite.

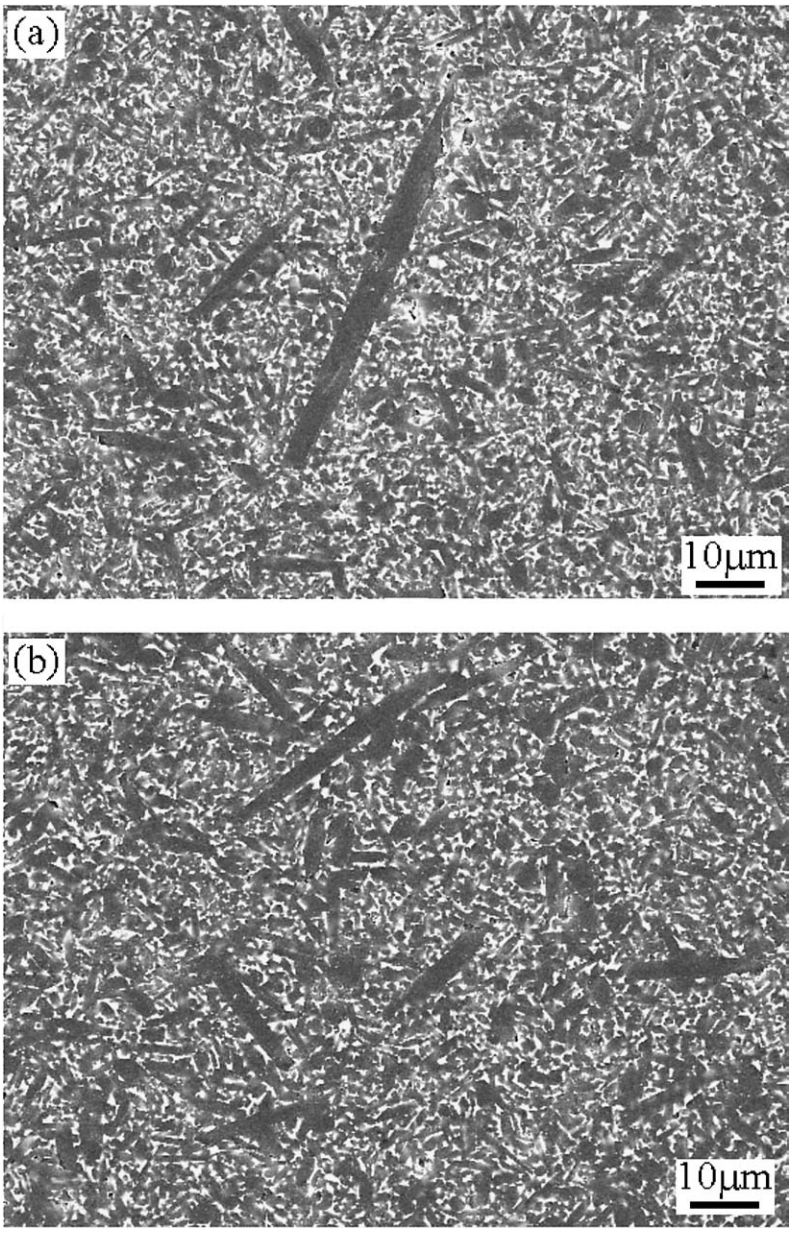

Figure 5 SEM photographs of polished and plasma-etched cross-sectional surfaces of sintered Si_3N_4-powder compacts at 1900°C with 6 h hold under a N_2 pressure of 1 MPa: (a) without and (b) with heat treatment at 1350°C for 8 h.

8 h. This shows that once the nitriding reaction completes, the prolonged holding time will not influence the pore structure. A decrease in the nitriding temperature increases the area density of Si_3N_4 nuclei [24], but decreases the reaction kinetics, so the formed products will quickly seal the channels and stops reaction, which results in a relatively low final extent of reaction and higher closed porosity. Thus, the difference in the open porosity between 1300 and 1350°C is not caused by the nitriding time, but the temperature. It is also observed that the densities of RBSN materials increase with increasing nitrided percent and this is in good agreement with the volume expansion of approximately 22% connected with the conversion of silicon to Si_3N_4. This expansion is taken up by the interstitial void between the particles in the compacts, resulting in pore filling and the increase of density.

It is found that the addition of Si_3N_4 powder to green bodies significantly reduces the density and increases the open porosity of nitride bodies. This indicates that

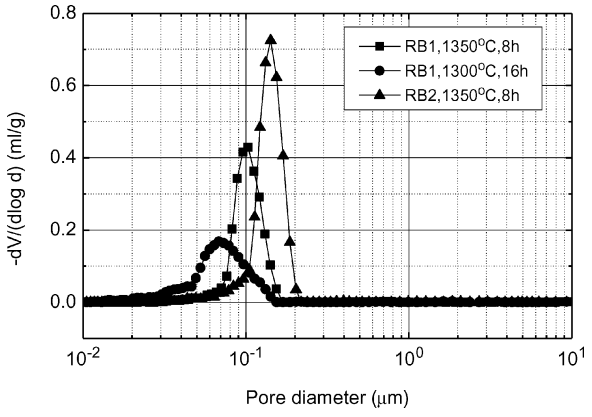

Figure 6 The pore size distribution of RBSN materials (RB1 materials nitrided at 1350°C for 8 h and 1300°C for 16 h, respectively, and RB2 materials nitrided at 1350°C for 8 h).

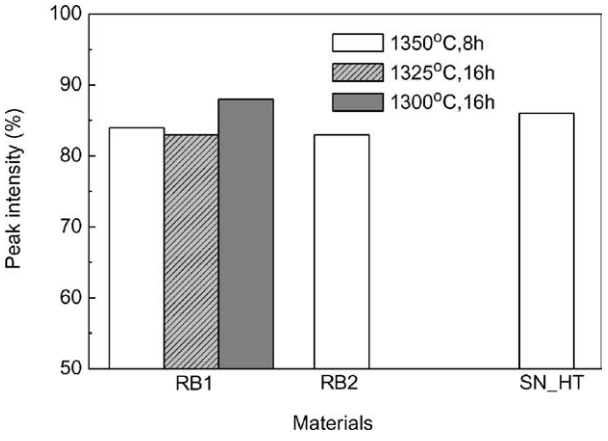

Figure 7 The strongest XRD peak intensity of crystalline $Yb_4Si_2O_7N_2$ phase present in the RB1 and RB2 materials obtained at various nitriding temperatures and Si_3N_4-powder compacts with heat treatment (SN_HT) at 1350°C for 8 h.

the addition of Si_3N_4 particles prevents the densification of Si compacts during nitridation. Since Si_3N_4 particles are fully reacted, they make no contribution to the densification of RBSN materials. In fact, they result in an increase of in internal porosity and a decrease in density because of the formation of an open network structure. Since no Si peaks are found in nitrided RB2 materials, the nitridation is considered to be complete at 1350°C. It is noted that the all RBSN materials show a very low content of β-phase (<2 wt%) and the addition of α-Si_3N_4 further decrease the β-phase content. The decrease in the β-phase content is attributed to the "seeding" effect of these α-Si_3N_4 additions, which promote α-nitride formation [25].

Fig. 6 shows the effect of the nitriding temperature and the addition of Si_3N_4 particles on the pore size distribution of RBSN materials. The average pore size of RB1 materials is 0.1 μm at 1350°C for 8 h, and 0.07 μm at 1300°C for 16 h, respectively. The RB1 materials obtained at 1300°C contain a wider pore size distribution than those obtained at 1350°C. In addition, although the density of the former is lower than the latter, the population of pores of approximately 0.06 μm in the former is much less than that the population of pores of ~0.1 μm in the latter. This is consistent with the relatively high population of close pores in the former. This means that the nitridation at lower temperature for a longer reaction time easily created finer micropores as well as closed pores. The average pore size shows a slightly increases from 0.1 to 0.15 μm due to the addition of Si_3N_4 particles to green compacts. Especially, the Si_3N_4 addition results in the increase of the population of relatively coarse pores and this is in good agreement with the open porosity data.

XRD analysis shows that only crystalline $Yb_4Si_2N_2O_7$ is observed as crystalline secondary phase in all RBSN materials. The formation of $Yb_4Si_2N_2O_7$ is attributed to the chemical reaction between Yb_2O_3, Si, and SiO_2 at the Si particle surface, and/or newly formed Si_3N_4 during the nitridation process. The amount of $Yb_4Si_2N_2O_7$ phase in these materials can be estimate by the strongest XRD peak intensities of this phase shown in Fig. 7. Because the Yb_2O_3 phase is not observed in all nitrided bodies, it can be considered to have completely converted into the crystalline $Yb_4Si_2N_2O_7$ phase during the nitridation process. Except the 1300°C-nitrided RB1 materials, no significant difference is found in the strongest XRD peak intensity of $Yb_4Si_2N_2O_7$ phase in the nitrided materials and treated Si_3N_4-powder compacts, which means that these materials contain almost the same amount of $Yb_4Si_2N_2O_7$ phase. The reason why the 1300°C-nitrided RB1 materials show a relatively high amount of $Yb_4Si_2N_2O_7$ phase is associated with the incomplete nitridation reaction and an especially high amount of residual Si. The $Yb_4Si_2N_2O_7$ phase is also the only crystalline secondary phase in the treated Si_3N_4-powder compacts in our model experiment. These results show that the formation of crystalline $Yb_4Si_2N_2O_7$ phase is almost independent of the properties of starting raw materials and even fabrication techniques. From the thermodynamic point of view, the $Yb_4Si_2N_2O_7$ phase may be the stablest phase in the system of Si_3N_4-SiO_2-Yb_2O_3.

Fig. 8 presents the microstructure of some typical RBSN materials. In addition to the micropores (<1 μm), there are some macropores (>1 μm) and even a few macropores of ~4 μm are visible in the microstructure shown in Fig. 8a, c and e. The size of these macrospores strongly depends on the size of the coarse particles in the starting Si powders; the coarser the starting Si powder used, the larger the size of these macropores [26]. SEM photograph presented in Fig. 1 indicates that the original Si powders cover a large distribution of particle size from fine particles <1 μm to coarse particles reaching diameters of about 5 μm. Moreover, XRD analysis shows that Si_3N_4 products in all RBSN materials consist basically of α-phase. It has been generally accepted that the formation of α-phase is attributed to the gas-phase reaction between Si vapour and molecular nitrogen through a vaporization/condensation type mechanism, similar to a CVD process [27, 28]. This reaction always takes place in a predominant nitrogen environment, and very often this will be outside the boundaries of the original Si particles, which leads to the formation of the pores at their original positions after complete reaction. It is

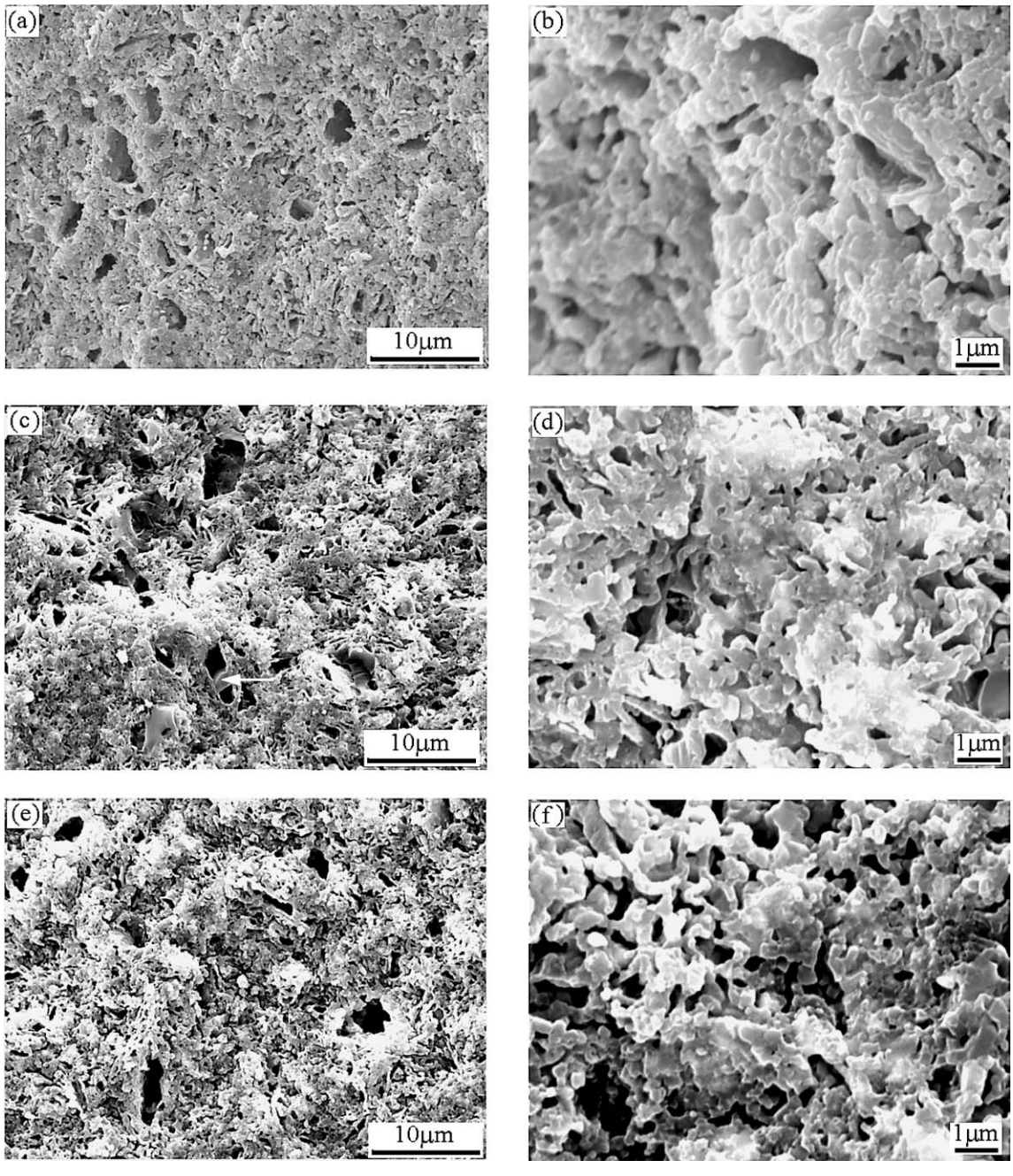

Figure 8 SEM photographs of facture surfaces of RBSN materials: (a) and (b) RB1 nitrided at 1350°C × 8 h, (c) and (d) RB1 nitrided at 1300°C × 16 h, (e) and (f) RB2 nitrided at 1350°C × 8 h ((a) (c) and (e) ×2500, (b) (d) and (f) ×10000).

clearly observed that the unreacted Si left inside such type of pores, as indicated by a white arrow in Fig. 8c, is due to the reaction stopping. Therefore, the formation of these "noticeable" macrospores is mainly associated with the direct evaporation of very coarse Si particles.

In addition to the porous structure, the Si_3N_4 grains are almost fine and equiaxed and XRD analysis shows that they are almost composed of α-phase. Obviously, these fine grains exist in agglomerated form. Because the nitriding reaction is highly exothermic, large temperature gradients can occur during RBSN formation if heat is generated faster than it is removed either by conduction through the sample or by transporting away from the external surfaces. Some authors have estimated the temperature rise during reaction and found that it could be over 100°C for the sample of ∼0.2 cm thickness during nitridation at 1350°C [29]. Furthermore, the temperature rise increases with increasing sample thickness. Because the thickness of Si green compacts is about 0.5 cm, the local temperature reaches above the melting point (1410°C) of Si occurs during nitridation at 1350°C, resulting in the coagulation of partly melted particles in the reaction system. It can be seen that the extent of agglomeration in nitridated RB1 materials at 1350°C (Fig. 8b) is apparently larger than those nitrided at 1300°C (Fig. 8d) as well as nitrided RB2 materials (Fig. 8f). In addition to lowering nitriding temperature, the extent of agglomeration can be effectively reduced by adding Si_3N_4 particles to green bodies, because the fully reacted Si_3N_4 reduce the chance of local overheating.

TABLE III Pressureless sintering of RBSN materials (nitriding condition: 1350°C for 8 h) at 1800°C for 6 h hold

Sample no.	BD (g/cm^3)	RD (%)	LS (%)	VS (%)	WL (%)
RB1	3.17	90.63	8.48	24.60	6.39
RB2	3.20	91.49	10.18	28.19	7.37
SN_HT[a]	3.24	92.54	17.90	45.86	10.53

[a]SN_HT = Si_3N_4-powder compacts with heat treatment at 1350°C for 8 h in our model experiment.

TABLE IV Gas-pressure sintering of RBSN materials at 1900°C for 6 h hold under a N_2 pressure of 1 MPa

Sample no.	Nitriding condition	BD (g/cm^3)	RD (%)	LS (%)	VS (%)	WL (%)
RB1	1300°C, 16 h	3.45	98.46	10.79	29.67	1.50
	1325°C, 16 h	3.35	95.65	9.81	26.58	4.24
	1350°C, 8 h	3.24	92.55	8.63	26.96	5.90
RB2	1350°C, 8 h	3.45	98.61	11.62	31.18	3.96
SN_HT	1350 °C, 8 h	3.44	98.18	18.69	47.83	5.62

3.3. Post-densification of RBSN materials

Pressureless and gas-pressure sintering results of RB1 and RB2 materials in all cases are summarized in Table III and IV, respectively. In order to compare with the sintering behavior of RBSN materials, the pressureless and gas-pressure sintering of Si_3N_4-powder compacts with heat treatment is correspondingly illustrated in Table III and IV and these samples are designated as SN_HT. All these materials show only ~91 % relative density by pressureless sintering at 1800°C, indicating incomplete densification. Moreover, RB2 and SN_HT materials are densified to more than 98% relative density by gas-pressure sintering at 1900°C. This means that the RB2 materials show almost the same densification behavior as the SN_HT materials. However, in comparison with the RB2 materials, the nitrided RB1 materials at the same condition show only 92.55% relative density by gas-pressure sintering, indicating a poor densification behavior. But, the 1300°C-nitrided RB1 materials are densified to more than 98% relative density, almost the same as the 1350°C-nitrided RB2 materials as well as SN_HT materials. The effect of nitriding temperature and Si_3N_4 additions on the post-densification of RBSN is further illustrated in Fig. 9. Gas-pressure sintering for all materials (RBSN materials and Si_3N_4-powder compacts) results in a small increase in the sintering shrinkage and a significant decrease in the weigh loss in comparison with the pressureless sintering. Generally, the weight loss of Si_3N_4 during sintering is due to the decomposition of Si_3N_4 or the formation of SiO gas, and higher N_2 pressure can suppress this volatilisation [30, 31]. The SN_HT materials show higher weight loss than the RBSN materials during sintering especially pressureless sintering due to the low starting density. In addition, the weight loss of the RBSN materials (RB1) decreases with the decrease of nitrided percent or the increase of residual Si content. Compared with Si_3N_4-powder materials (SN_HT), The RBSN materials shows a smaller sintering shrinkage and this is due to the higher starting density.

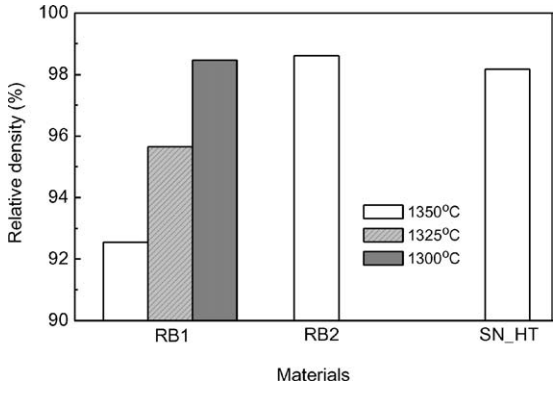

Figure 9 Effect of the nitriding temperature and Si_3N_4 addition on the relative density of sintered RBSN materials at 1900°C with 6 h hold under a N_2 pressure of 1 MPa.

Fig. 10 gives the typical microstructures of GPSed-RBSN materials (SRBSN) at 1900°C. Many pores are visible in Fig. 10a, but very few pores can be observed in Fig. 10b and c. These SRBSN materials show the similar microstructures composed of small matrix grains and elongated β-Si_3N_4 grains. But, the grain growth of elongated β-Si_3N_4crystals in Fig. 10a and b is more noticeable than in Fig. 10c and this is associated with the relatively low β-phase content in the nitrided RB2 materials. XRD analysis of all SRBSN materials reveals that the α-to-β phase transformation is complete during sintering.

4. Discussion

4.1. Effect of crystalline secondary phases

Concerning the liquid phase sintering, the effect of the pre-formation of crystalline secondary phases on the densification may be caused by the amounts, viscosity, surface tension and especially distribution of liquid phase throughout the samples. According to the theory of phase-equilibrium diagrams, for a given composition, the formation of liquid phase is strongly dependent on the temperature, but independent of heating history or heating process. In order to interpret this argument, Fig. 11 illustrates a schematic representation of the phase diagram of a typical two-component system with a stable compound. For a starting composition of a mixture A and B corresponding to point Xo, let us consider two routes to heat the mixture to temperature T_2 to examine the formation of liquid under equilibrium condition. One is that the system is directly heated to T_2 at which phase B dissolves and disappears, the liquid with composition of X_K forms and coexists with phase A. The amount of liquid is determined by the lever rule. The other is that the system is first heated to T_1 and then cooled to room temperature. Thus, phase B disappears and crystalline C is formed during this heating process. The new system is composed of A and C and its overall composition is still located at point Xo, provided that the material loss is neglected during the heating process. Then, the new system is heated to T_2 at which crystalline C dissolves and disappears, the liquid forms and coexists with phase A. The composition of liquid in the new system at T_2 is still located at X_K and its amount should be the same as that of the system without heat treatment. Obviously, although the melting point of crystalline C

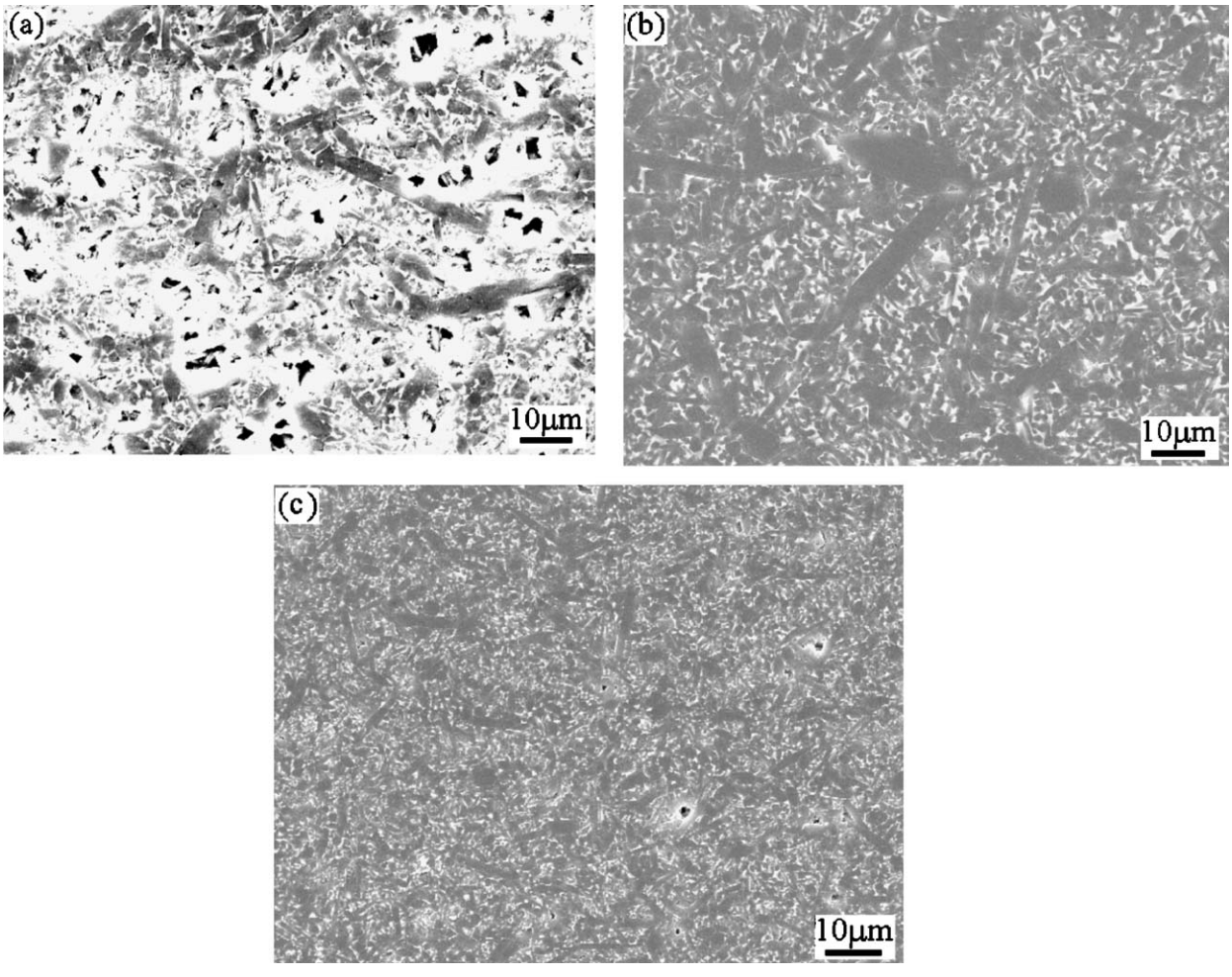

Figure 10 SEM photographs of polished and plasma-etched cross-sectional surfaces of sintered RBSN materials at 1900°C with 6 h hold under a N_2 pressure of 1 MPa: (a) RB1 (nitrided at 1350°C × 8 h), (b) RB1 (nitrided at 1300°C × 16 h) and (c) RB2 (nitrided at 1350°C × 8 h).

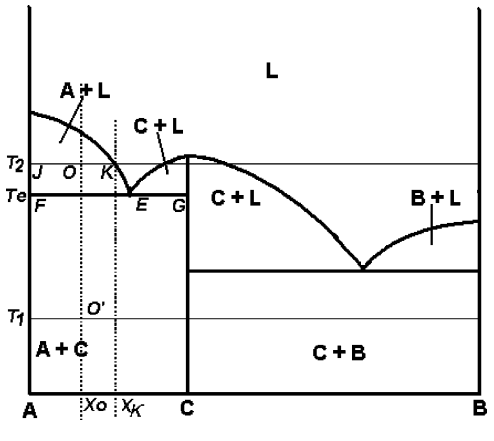

Figure 11 The phase diagram of a typical two-component system with a stable compound.

is higher than T_2, it completely dissolves and takes part in the formation of liquid at T_2. This means that under the equilibrium condition, the composition and properties of liquid is not related to the presence of crystalline C resulting from additional heat treatment, but only to the composition of the system and temperature. Accordingly, this argument can be analogical to the three (or even four)-component system.

As discussed above, it is concluded that for a fixed composition and temperature, the pre-formation of crystalline secondary phases does not affect the formation of liquid phase including composition, structure and properties, such as viscosity and surface tension, but might result in the local distribution of liquid throughout the sample during sintering. However, the same sintering behavior between the untreated and treated Si_3N_4-powder compacts clearly shows that the pre-formation of crystalline secondary phases does not result in the localized distribution of liquid, because a homogenization of locally formed liquid occurs due to capillary force during sintering. All materials are densified to more than 90% relative density by pressureless sintering at 1800°C and this demonstrates that the crystalline secondary phases do not influence the formation of liquid phase. The 1300°C-nitrided RB1, 1350°C-nitrided RB2 and SN_HT materials all are sintered to more than 98% relative density at 1900°C, as shown in Fig. 9. This means that the crystalline $Yb_4Si_2N_2O_7$ in RBSN does not influence the post-densification. Although the 1350°C-nitrided RB1 materials shows a poor densification behavior, this should not be attributed to the presence of crystalline $Yb_4Si_2N_2O_7$, because all these materials contain almost the same amount of $Yb_4Si_2N_2O_7$, as shown in Fig. 7. In particular, crystalline $Yb_4Si_2N_2O_7$ can completely melt at sintering temperature of 1900°C, higher than its melting point of 1870°C. In fact, the lowest eutectic temperature in the system of Si_3N_4-SiO_2-Yb_2O_3-MgO

should be less than 1660°C, which is the lowest eutectic temperature of the SiO_2-Yb_2O_3 system, and even 1350°C. Moreover, the complete dissolution of crystalline $Yb_4Si_2N_2O_7$ phase is not related to its melting point, but only to the starting composition of the system. Some authors' work [23] using Y_2O_3-Al_2O_3 as sintering additives also clearly demonstrated that the untreated materials showed the same sintering and α-to-β phase transformation behavior as the treated materials at 1450°C for 10 h, which leaded to the presence of crystalline $Y_2Si_2O_7$. However, the sintering of the treated materials at the same condition in the presence of carbon was retarded below 1750°C and this is attributed to the change of the composition due to the carbothermal reduction process, which is evident in the shift of crystalline secondary phase from $Y_2Si_2O_7$ to $Y_{10}Si_6O_{24}N_2$. The change of composition result in the change in composition and properties of liquid, thereby affecting the sintering behavior, but this effect has no close relationship with the presence of crystalline $Y_{10}Si_6O_{24}N_2$. Therefore, their work is in excellent agreement with our present argument. Thus, the reason why the pre-formation of crystalline secondary phases does not affect the liquid sintering of ceramic powders has been explained. The role of crystalline secondary phases in the post-densification of RBSN has also been clarified in this work.

4.2. Effect of residual Si

Usually, when Si peaks are not detected by XRD, the nitridation is considered to be nearly complete. However, a small amount of unreacted Si always exists in the "fully" nitrided bodies and can be detected by other techniques, such as STEM/EDX microanalysis [3]. This residual Si cannot be nitrided at nitriding temperature lower than its melting points (1410°C). That is to say, the residual Si in RBSN cannot be avoided. Hence, the effect of residual Si on the post-densification should be considered and understood. Fig. 9 shows that the relative density of sintered RB1 materials increases with the decrease of nitriding temperature. This means that the post-densification of RBSN is promoted by the decreased nitriding temperature.

Based on the argument for thermal decomposition of Si_3N_4, Baik *et al*. [32] added a few weight percent pure Si to obtain fully dense MgO-doped Si_3N_4 ceramics under an atmosphere of N_2 pressure, because the presence of free Si maintains high silicon activity in the secondary glass phase through which mass transport occurs and keeps N_2 pressure low so that net-driving force for sintering remains positive. Although a higher N_2 pressure (usually 1–10 MPa) has been widely used to suppress the decomposition and promote the densification of Si_3N_4 at higher temperature ($\geq$1900°C), the presence of free Si should further suppress the decomposition by decreasing the equilibrium partial pressure of N_2. It is evident that the weight loss decreases as the residual Si content increases in RBSN bodies, which means that the residual Si contributes to the weight gain by the nitridation of Si during post-sintering. Because the solubility of N_2 in liquid Si is fairly high, liquid Si encourages fast diffusion of N_2 and reaction sites are easily created. Hence, the residual Si in RBSN will convert into β-Si_3N_4 by liquid-gas reaction during post-sintering [27].

To understand the nitridation of residual Si during post-sintering, the sintering of 1300°C-nitrided RB1 material was also performed at 1900°C for 2 h. The residual Si is not observed in sintered bodies any more, whereas they reach only ~93% relative density. In contrast, this RB1 material can be sintered to more than 98% relative density at 1900°C for 6 h, as shown in Table IV. It seems that the residual Si in RBSN shows no significant contribution to the post-densification. Despite this, the residual Si does no harm to the post-densification of RBSN. The work of other authors also supports this conclusion [10].

However, it must be emphasized that too much residual Si is detrimental to the post-densification. Because of the poor wetting ability of Si_3N_4 particles by liquid Si [33], the molten Si droplets coagulate and are squeezed out of the body along the open pore channels. This phenomenon was observed in our work. If too much unreacted Si exists in RBSN, although most changes into Si_3N_4 during post-sintering, some still remain in the final products, which lead to degradation of mechanical properties [10, 34]. In order to obtain Si_3N_4 materials with good properties, the nitridation should be completed, that is, the residual Si in RBSN should be reduced to the least level.

4.3. Effect of pore size distribution

Kleebe *et al*. [5, 13] stressed that the micropore size distribution of RBSN has a strong influence on the densification and finer micropores enhance densification. However, this effect was not observed in our work. Although the nitrided RB1 materials at 1350°C have slight finer average pore diameter (~0.1) than the nitrided RB2 materials at this temperature, the former shows poor densification behavior. Being aware that the RB2 materials contain relatively high open porosity, it could be suggested that this difference was caused by the population of open pores. However, this suggestion is not consistent with the RB1 materials with finer pores and higher closed porosity reaching more than 98% relative density during post-sintering. The size of the large pores in the RBSN bodies in the present work is about 5 μm, but they can be removed during post-sintering, as shown in Fig. 10b and c. The elimination of these large pores is associated with a combination of liquid filling and grain growth arising from the dissolution-reprecipitation process. Since all RBSN materials almost contain the same fraction of these macropores due to the same starting Si particles, the poor densification of the nitrided RB1 materials at 1350°C cannot also be attributed to the presence of the "noticeable" macropores. Therefore, the effect of pore size distribution on the densification of RBSN was not demonstrated in the present work.

4.4. Effect of agglomerates

Because the grain size of the RB1 materials nitrided at 1350°C is almost the same as that of those nitrided at

1300°C and RB2 materials, the grain size effect on their densification should be excluded. As discussed previously, the poor densification behavior of the nitrided RB1 materials at 1350°C should be attributed to the highly agglomerated structure. The liquid phase sintering of Si_3N_4 ceramics is described by rearrangement, solution-diffusion-precipitation, and coalescence [34]. Once the liquid phase forms in the initial stage of sintering, the particle rearrangement will occur and densification will start under the capillary force. In order to explain the effect of agglomerates on the densification, we should consider a basic presumption that the large particles or agglomerates must undergo a disintegration process due to the penetration of the liquid phase prior to rearrangement, because some small particles can rearrange more readily than the large particles and lead to a more efficient particle packing [36–38]. More importantly, the small particles are more beneficial to the solution-diffusion-precipitation process, which is critical for densification, because the finer particles have a higher solubility in liquid than large particles. XRD analysis shows that the α-to-β phase transformation for all RBSN materials during post-sintering is complete. However, the α-to-β transformation has been commonly believed to occur in the presence of liquid phase, because no evidence of this transformation occurrence without the help of the solution-precipitation mechanism has been found to date. Therefore, this presumption sounds reasonable and easily understood.

The penetration rate of liquid into the particle interstices can be estimated by the following formula [35]:

$$X^2 = \frac{r\gamma t \cos\theta}{2\eta} \tag{3}$$

where X is the depth of penetration, r is the radius of capillary tube, γ and η is the specific surface energy and viscosity of the liquid, respectively, θ is the wetting angle. According to Equation 3, for a given liquid, the disintegration process strongly depends on

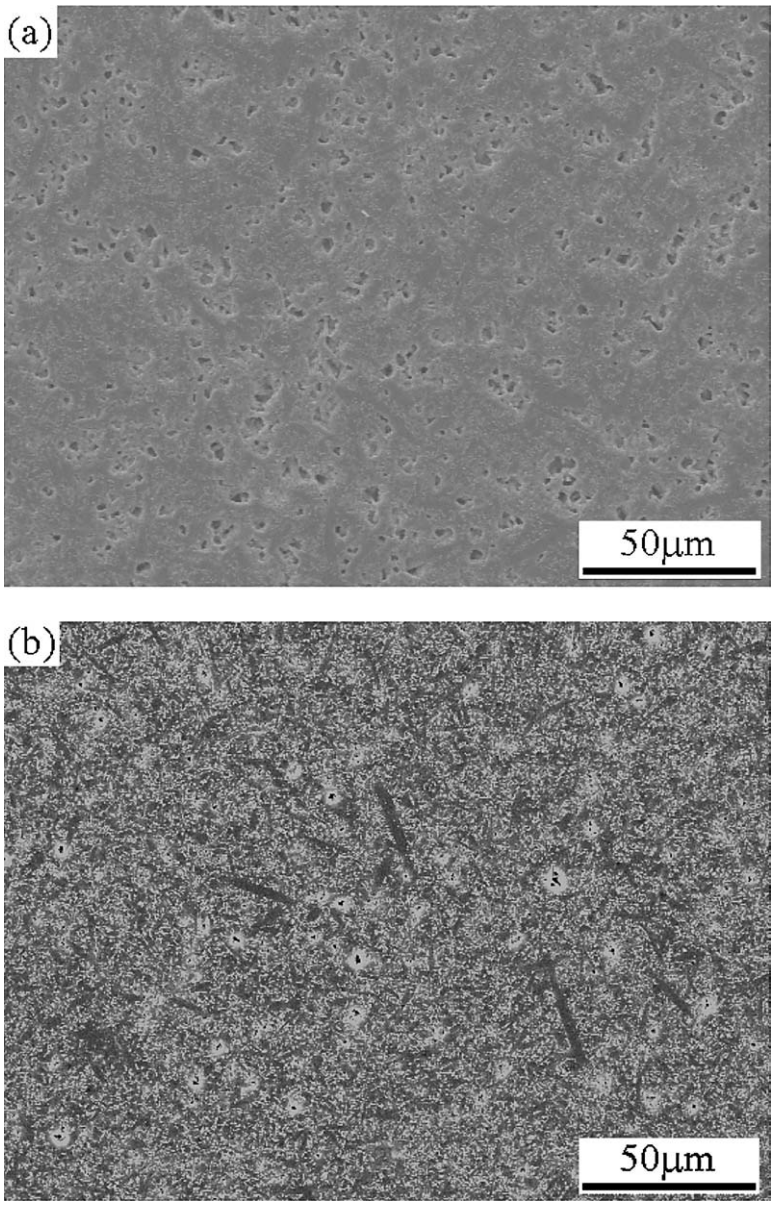

Figure 12 SEM photographs of polished and plasma-etched cross-sectional surfaces of (a) sintered RB1 nitrided at 1350°C and (b) sintered Si_3N_4-powder compacts by pressureless sintering at 1800°C.

the particle interstice size. This indicates that loose and small agglomerates are disintegrated more quickly than the dense and large agglomerates. The liquid viscosity often decreases by orders of magnitude with increasing temperature, so the higher sintering temperature can greatly accelerate the disintegration process. More importantly, the disintegration process strongly depends on the size of agglomerates. It is easily understood that the smaller the agglomerates are, the shorter is the time of complete disintegration.

Biswas *et al*. [39] observed that the solution-reprecipitation process during sintering of Si_3N_4 is a diffusion–controlled process governed by the following equation [35]:

$$\frac{\Delta L}{L_0} = \frac{1}{3}\frac{\Delta V}{V_0} = \left(\frac{6k_2\delta DC_0V_0\gamma_{LV}}{k_1RT}\right)^{\frac{1}{3}} r^{-\frac{4}{3}} t^{\frac{1}{3}} \quad (4)$$

where δ is the boundary thickness, γ_{LV} is the liquid-vapor surface tension, k_1 is the ratio of pore and particle radius, k_2 is the constant of proportionality, D is the diffusion coefficient of the solid atoms in the liquid grain boundary, r is the particle size, t is the time, R is the gas constant, T is the absolute temperature. According to Equation 4, for a fixed liquid and temperature, the densification rate during solution-precipitation process strongly depends on the particle size (r), k_1 and the boundary thickness (δ). The smaller the k_1 and δ are, the faster the densification rate is. When the size and amounts of agglomerates in the green bodies is smaller and lower, they can be quickly disintegrated and homogenously rearranged in the presence of liquid phase. Thus, densification behavior is uniform throughout the sample. When the size and mounts of agglomerates is larger and higher, they cannot be quickly disintegrated and inhomogeneously rearranged. Thus, a localized nonuniform densification will occur and results in the formation of a strong porous skeleton structure, which is difficult to remove by liquid filling and grain coarsening in the absence of sufficient liquid phase.

The effect of agglomerates on the post-densification of RBSN during pressureless sintering at 1800°C is not obvious because of their incomplete densification, but become apparent during gas-pressure sintering at 1900°C. This shows that a strong porous microstructure arising from the localized non-uniform shrinkage due to highly agglomerate cannot be removed in spite of the use of a higher temperature and a higher pressure of N_2. The effect of the agglomerates on the liquid phase sintering was also reported in the sintering of W-Cu nanocomposite powder [40]. Fig. 12 shows the microstructure of the sintered RB1 materials nitrided at 1350°C and sintered Si_3N_4-powder compacts by pressureless sintering at 1800°C. The former is considered to be highly agglomerated (as shown in Fig. 8a and b), but the latter is less agglomerated (as shown in Fig. 3) before sintering. It is very evident that the former shows a coarser porous structure (Fig. 12a), but the latter shows a finer porous structure (Fig. 12b). The latter can be further densified due to the lower viscosity and higher amount of liquid under a higher temperature, but the former is difficult to be further densified due to a coarse porous network structure. Therefore, it is suggested that the control of the agglomerates in the microstructure of RBSN is very important to post-densification.

5. Conclusions

(a) The pre-formation of the crystalline secondary phases does not influence the sintering of Si_3N_4-powder compacts and also does not result in the abnormal grain growth, because they do not affect the formation and distributed homogenization of liquid phase during sintering at higher temperature. The composition and properties of liquid are dependent on the composition of the system and temperature, but independent of the presence of crystalline secondary phases. Furthermore, no effect of crystalline secondary phase in RBSN on the post-densification has been clearly demonstrated.

(b) The residual Si and pore size distribution show no significant effect on the post-densification of RBSN. Although some large pores about 5 μm in size are present in the RBSN bodies due to large original Si particles, they can be eliminated during post-sintering. The small amount of residual Si will convert into Si_3N_4 and result in the weight gain by nitridation of liquid Si during post-densification, but too much residual Si become detrimental to the post-densification, because the molten Si droplets coagulate and are squeezed out of the body along the open pore channels due to the poor wetting ability of Si_3N_4 particles by liquid Si.

(c) The post-densification of RBSN was found to be strongly dependent of the agglomerates present in the microstructure. The effect of agglomerates on the post-densification is controlled by the amounts and size of agglomerates, especially the size of agglomerates. The larger size and higher amounts of agglomerates result in coarser porous structure and prevent further densification, while the smaller size and lower amounts of agglomerates do not influence the post-densification because they can be quickly disintegrated and uniformly rearranged in the presence of liquid. The degree of agglomeration of RBSN can be effectively reduced by adding Si_3N_4 powder to green bodies or lowering the nitriding temperature, which leads to a nearly complete densification.

Acknowledgements

The authors wish to express special thanks to the reviewer for the recommendation of reference 23 (*J. Amer. Ceram. Soc*. **85**(1) (2002) 245–252).

References

1. J. A. MANGELS and G. J. TENNENHOUSE, *Amer. Ceram. Soc. Bull*. **59**(12) (1980) 1216, 1222.
2. J. A. MANGELS, Report Prepared for NASA-Lewis, Contract No. DEN 3-167, November (1980).
3. L. K. L. FALK, R. POMPE and G. L. DUNLOP, *J. Mater. Sci*. **20** (1985) 3545.
4. G. ZIEGLER, J. HEINRICH and G. WÖTTING, *ibid*. **22** (1987) 3041.
5. H. J. KLEEBE and G. ZIEGLER, *J. Amer. Ceram. Soc*. **72**(12) (1989) 2314.

6. T. N. TIEGS, J. O. KIGGANS and Z. L. PLOETZ, *Ceram. Eng. Sci. Proc.* **14**(1–2) (1993) 378.
7. T. N. TIEGS, J. O. KIGGANS, F. C. MONTGOMERY, H. T. LIN, D. L. BARKER, J. D. SNODGRASS, E. M. SABOLSKY and D. W. COFFEY, *ibid.* **17**(3) (1996) 354.
8. S. Y. LEE, K. AMOAKO-APPIAGYEI and H. D. KIM, *J. Mater. Res.* **14**(1) (1999) 178.
9. B. T. LEE, J. H. YOO and H. D. KIM, *Mater. Trans. JIM* **41**(2) (2000) 312.
10. B. T. LEE, J. H. YOO and H. D. KIM, *Mater. Sci. Eng.* A **333** (2002) 306.
11. F. L. RILEY, *J. Amer. Ceram. Soc.* **83**(2) (2000) 245.
12. K. NEGITA, *J. Mater. Sci. Lett.* **4** (1985) 417.
13. H. J. KLEEBE, G. WÖTTING and G. ZIEGLER, *Sci. Ceram.* **14** (1988) 407.
14. T. NISHIMURA and M. MITOMO, *J. Mater. Res.* **10**(2) (1995) 240.
15. W. DRESSLER, H. J. KLEEBE, M. J. HOFFMANN, M. RUHLE and G. PETZOW, *J. Euro. Ceram. Soc.* **16** (1996) 3.
16. H. HAYASHI, K. HIRAO, M. TORIYAMA and S. KANZAKI, *J. Amer. Ceram. Soc.* **84**(12) (2001) 3060.
17. H. HAYASHI, K. HIRAO, M. KITAYAMA, Y. YAMAUCHI and S. KANZAKI, *J. Ceram. Soc. Jpn.* **109**(12) (2001) 1046.
18. H. PARK, H. E. KIM and K. NIIHARA, *J. Amer. Ceram. Soc.* **80**(3) (1997) 750.
19. S. GUO, N. HIROSAKI, T. NISHIMURA, Y. YAMAMOTO and M. MITOMO, *Philosophical Magazine* A, **82**(16) (2002) 3027.
20. H. YOKOTA and M. IBUKIYAMA, *J. Amer. Ceram. Soc.* **86**(1) (2003) 197.
21. W. H. LEE and H. E. KIM, *ibid.* **80**(10) (1997) 2737.
22. R. G. PIGEON and A. VARMA, *J. Mater. Sci. Lett.* **11** (1992) 1370.
23. H. D. KIM, B. D. HAN, D. S. PARK, B. T. LEE and P. F. BECHER, *J. Amer. Ceram. Soc.* **85**(1) (2002) 245.
24. A. ATKINSON, A. J. MOULSON and E. W. ROBERTS, *ibid.* **59**(7–8) (1976) 285.
25. O. J. GREGORY and M. H. RICHMAN, *J. Mater. Sci. Lett.* **3** (1984) 112.
26. J. HEINRICH and G. STREB, *J. Mater. Sci.* **14** (1979) 2083.
27. H. M. JENNINGS, *ibid.* **18** (1983) 951.
28. R. G. PIGEON, A. VARMA and A. E. MILLER, *ibid.* **28** (1993) 1919.
29. B. W. SHELDON, J. SZEKELY and J. S. HAGGERTY, *J. Amer. Ceram. Soc.* **75**(3) (1992) 677.
30. F. F. LANGE, *ibid.* **65**(8) (1982) C-120.
31. C. GRESKOVICH and S. PROCHAZKA, *ibid.* **64**(7) (1981) C-96.
32. S. BAIK and R. RAJ, *ibid.* **68**(5) (1985) C-124.
33. J. C. SWARTZ, *ibid.* **59**(5–6) (1976) 272.
34. B. T. LEE and H. D. KIM, *J. Mater. Sci.* **34** (1999) 6169.
35. W. D. KINGERY, *J. Appl. Phys.* **30**(3) (1959) 301.
36. W. J. HUPPMANN, H. RIGGER and G. PETZOW, in "Sintering-New Development ", edited by M. M. Ristić (Elsevier Scientific, Amsterdam, 1979) p. 272.
37. S. PEJOVNIK, D. KOLAR, W. J. HUPPMANN and G. PETZOW, in "Sintering-New Development" edited by M. M. Ristić (Elsevier Scientific, Amsterdam, 1979) p. 285.
38. W. J. HUPPMANN and G. PETZOW, in "Sintering Process", edited by G. C. Kuczynski (Plenum Press, New York, 1980) p. 189.
39. S. K. BISWAS and F. L. RILEY, *J. Amer. Ceram. Soc.* **86**(2) (2003) 212.
40. E. S. YOON, J. S. LEE, S. T. OH and B. K. KIM, *Int. J. Refract. Met. H.* **20** (2002) 201.

Received 16 July 2003
and accepted 11 May 2004